Microscopic spin-phonon coupling constants in $CuGeO_3$

Ralph Werner and Claudius Gros
Institut für Physik, Universität Dortmund, D-44221 Dortmund, Germany

Markus Braden
Forschungszentrum Karlsruhe, Institut für Nukleare Festkörperphysik, Postfach 3640, D-76021 Karlsruhe, Germany and Laboratoire Léon Brillouin (CEA-CNRS), Centre d'Études Nucléaires de Saclay, 91191 Gif-sur-Yvette Cédex, France

(Received 28 September 1998; revised manuscript received 22 December 1998)

Using random-phase approximation results, mean-field theory, and refined data for the polarization vectors we determine the coupling constants of the four Peierls-active phonon modes to the spin chains. We then derive the values of the coupling of the spin system to the linear ionic displacements, the bond lengths and the angles between bonds. Our values are consistent with microscopic theories and various experimental results. We discuss the applicability of static approaches to the spin-phonon coupling. The *c*-axis anomaly of the thermal expansion is explained. We give the values of the coupling constants in an effective one-dimensional Hamiltonian. [S0163-1829(99)07921-7]

I. INTRODUCTION

With the discovery of the first inorganic spin-Peierls compound $CuGeO_3$,[1] it has become possible to investigate the physics of the spin-Peierls transition in quasi-one-dimensional spin chains with high precision. As a consequence, it has attracted much attention both in experiment and theory. Yet, for a long time the absence of a soft phonon mode[2,3] has been puzzling, since the behavior was believed not to be consistent with the standard approach to spin-Peierls transitions by Cross and Fisher.[4] The frequencies of the Peierls-active phonon modes being of the order of the magnetic exchange,[5] it has been argued that the Cross and Fisher approach is not applicable because of the nonadiabacity of the phonons.[6] Only recently we were able to show[7] that the random-phase-approximation (RPA) approach by Cross and Fisher indeed is consistent with the hardening of the Peierls-active phonon modes.[5]

It is now tempting to combine the RPA results with the detailed data on the phonons acquired by Braden *et al.*[5] Treating the lattice with the standard harmonic theory and including the spin-phonon coupling mean-field like, we calculate the microscopic coupling constants between the lattice and the spin chains. It is then possible to predict the effect of structural changes on the spin system, namely the antiferromagnetic exchange *J*. The latter has been subject to various experimental[8–10] and theoretical studies.[11–17]

The microscopic three-dimensional (3D) Hamiltonian we have to consider consists of three parts:

$$H = H_s + H_p + H_{sp}. \tag{1}$$

The Heisenberg spin Hamiltonian

$$H_s = J\sum_{\mathbf{l}} \mathbf{S}_{\mathbf{l}}\cdot\mathbf{S}_{\mathbf{l}+\hat{z}} + J_2\sum_{\mathbf{l}} \mathbf{S}_{\mathbf{l}}\cdot\mathbf{S}_{\mathbf{l}+2\hat{z}} \tag{2}$$

with the exchange integrals J and J_2 between nearest-neighbor (NN) and next-nearest-neighbor (NNN) Cu *d* orbitals, respectively.

Further we distinguish the phonon part

$$H_p = \sum_{\substack{\mathbf{n}\\ \nu,\alpha}} \frac{(p^{\alpha}_{\mathbf{n},\nu})^2}{2m_\nu} + \sum_{\substack{\mathbf{n},\mathbf{n}'\\ \nu,\nu',\alpha,\alpha'}} \Phi^{\alpha,\alpha'}_{\mathbf{n},\mathbf{n}',\nu,\nu'} r^{\alpha}_{\mathbf{n},\nu} r^{\alpha'}_{\mathbf{n}',\nu'}, \tag{3}$$

describing the lattice vibrations in the harmonic approximation, where $\mathbf{r}_{\mathbf{n},\nu} = (r^x_{\mathbf{n},\nu}, r^y_{\mathbf{n},\nu}, r^z_{\mathbf{n},\nu})$ are the deviations from the ionic equilibrium positions.

Finally the spin-phonon coupling term reads

$$H_{sp} = \sum_{\mathbf{l}} \Delta J_{\mathbf{l},\mathbf{l}+\hat{z}} \mathbf{S}_{\mathbf{l}}\cdot\mathbf{S}_{\mathbf{l}+\hat{z}} + \sum_{\mathbf{l}} \Delta J_{\mathbf{l},\mathbf{l}+2\hat{z}} \mathbf{S}_{\mathbf{l}}\cdot\mathbf{S}_{\mathbf{l}+2\hat{z}}. \tag{4}$$

The energy scale $\Delta J_{\mathbf{l},\mathbf{l}+\hat{z}}$ is a function of the variation of the magnetic exchange integral with the atomic displacements $g^{\alpha}_{\mathbf{l},\nu} = \partial J/\partial r^{\alpha}_{\mathbf{l},\nu}$ to be discussed in Sec. III. The NNN term $\Delta J_{\mathbf{l},\mathbf{l}+2\hat{z}}$ is a function of $\partial J_2/\partial r^{\alpha}_{\mathbf{l},\nu}$.

The indices used are $\mathbf{n} = (n_x, n_y, n_z) \in \mathcal{Z}^3$ running over all unit cells of the three-dimensional crystal, the Cu-site index $\mathbf{l} = (l_x, l_y, l_z) \in \mathcal{Z}^3$ (two Cu sites per unit cell), and the unit vectors $\hat{x} = (1,0,0)$, $\hat{y} = (0,1,0)$, and $\hat{z} = (0,0,1)$ to nearest-neighbor unit cells in the corresponding direction. The index ν labels the 10 atoms within a unit cell as shown in Fig. 1 and $\alpha \in \{x,y,z\}$ is the vectorial component of the indexed quantity in the respective three-dimensional space.

In Sec. II we briefly summarize the diagonalization of the phonon Hamiltonian (3) followed by the discussion of the symmetry of the four Peierls-active phonon modes, including refined data for their polarization vectors. Using these symmetries we transform in Sec. III the microscopic spin-phonon coupling Hamiltonian (4) to normal coordinates in reciprocal space. This procedure yields relations between the different linear, angular, and normal mode coupling constants. Using RPA results and mean-field theory in Sec. V we obtain nu-

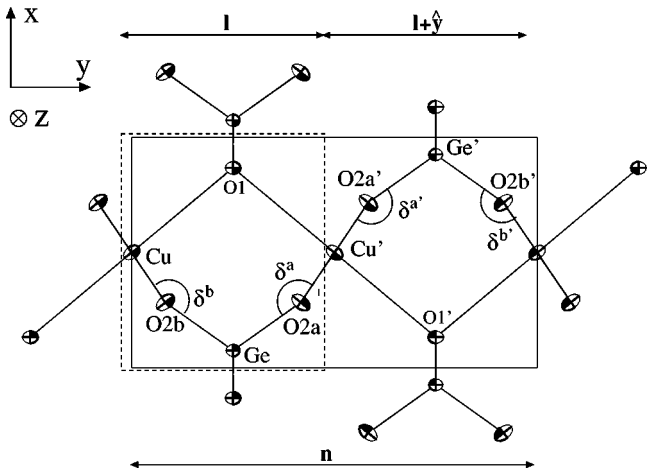

FIG. 1. Projection of the unit cell of $CuGeO_3$ on the *x*-*y* plane. The oxygen atoms are distinguished into O(1), O(2a), and O(2b), the atoms of the second formula unit are labeled with a prime. Each unit cell contains two Cu chains in the *z* direction (the positive *z* direction is into the plane). The broken lines show the reduced unit cell introduced in Sec. III. **n** is the index for the whole cells, **l** indexes the reduced cells.

merical values for the normal mode coupling constants which then can be converted to the real-space coupling constants. The resulting dependence of the magnetic exchange on static distortion of the lattice is discussed in Sec. VII and compared with values from the literature. Finally we derive an effective one-dimensional model to give coupling constants consistent with frequently applied theoretical approaches. The consistency of the different results gives a *a posteriori* justification of the mean-field approach.

II. PEIERLS-ACTIVE PHONON MODES

In the standard treatment of harmonic lattice dynamics, the initial problem of $3 \cdot N \cdot N_{\text{ion}}$ degrees of freedom (N number of unit cells, N_{ion} number of ions in the unit cell) is transformed into reciprocal space by a Fourier transformation, where N wave vectors fulfill the periodic boundary condition.[18] For any fixed wave vector one obtains a $3 \cdot N_{\text{ion}}$-dimensional problem which may be diagonalized, resulting in a set of $3 \cdot N_{\text{ion}}$ eigenmodes labeled by $\lambda \in \{1, \ldots, 3N_{\text{ion}}\}$. For, that purpose, the displacement and momentum operators are decomposed into eigenmode contributions introducing normal coordinates Q and conjugated momenta P:

$$\mathbf{r}_{\mathbf{n},\nu} = \frac{1}{\sqrt{N}} \sum_{\mathbf{q}} e^{i\mathbf{q}\mathbf{R}_{\mathbf{n}}} \sum_{\lambda} \frac{\mathbf{e}_{\nu}(\lambda,\mathbf{q})}{\sqrt{m_{\nu}}} Q_{\lambda,\mathbf{q}}, \tag{5}$$

$$\mathbf{p}_{\mathbf{n},\nu} = \frac{1}{\sqrt{N}} \sum_{\mathbf{q}} e^{i\mathbf{q}\mathbf{R}_{\mathbf{n}}} \sum_{\lambda} \mathbf{e}_{\nu}(\lambda,\mathbf{q}) \sqrt{m_{\nu}} P_{\lambda,\mathbf{q}}. \tag{6}$$

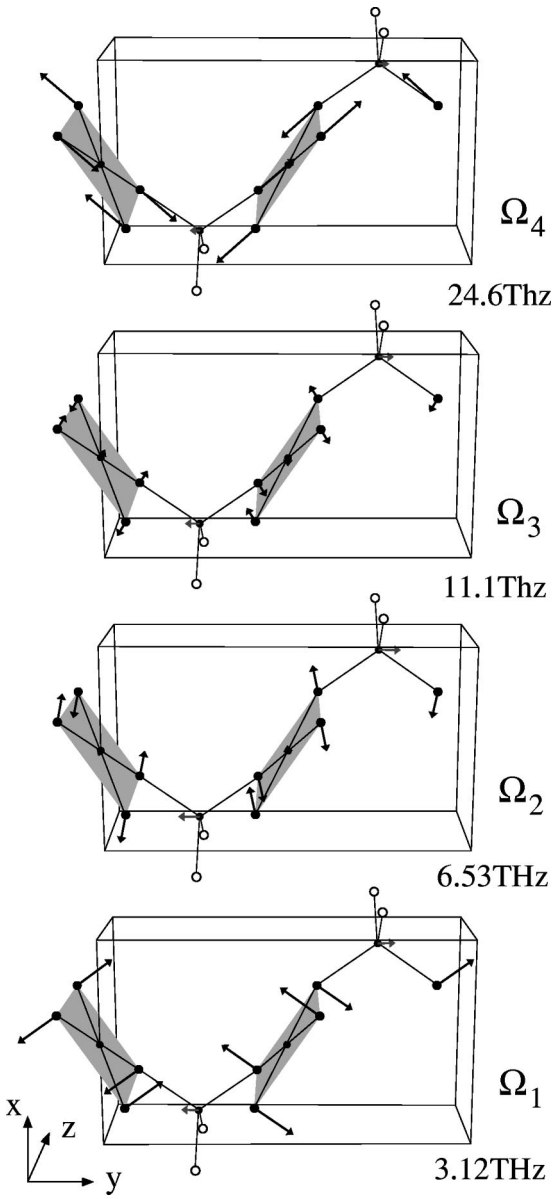

FIG. 2. Geometry of the T_2^+ eigenmodes as given by the polarization patterns in Table I. The shaded areas are the CuO_4 plaquettes which form the Cu chains in the *z* direction. The Cu atoms are in the center of each plaquette, the corners are formed by O(2) ions. The O(1) atoms are represented by the open circles with the Ge ions in between them. (Compare with the *x*-*y* projection given in Fig. 1.) Note that the O(2) elongations are in the *x*-*y* plane, the (small) Cu displacements are along the *z* axis, while the Ge displacements are along *y*.

The vectors $\mathbf{R}_{\mathbf{n}}$ designate the coordinates of the unit-cell origins. m_{ν} is the mass of the νth atom and $\mathbf{e}_{\nu}$ are polarization vectors. Note that we use a nonstandard definition for $\mathbf{R}_{\mathbf{n}}$ and $\mathbf{e}_{\nu}(\lambda,\mathbf{q})$ which will simplify the interpretation of the polarization vectors at high symmetry points in the Brillouin zone. Further transformation to boson creation and annihilation operator representation via

$$Q_{\lambda,\mathbf{q}} = \sqrt{\frac{\hbar}{2\Omega_{\lambda,\mathbf{q}}}} (b^{\dagger}_{\lambda,-\mathbf{q}} + b_{\lambda,\mathbf{q}}), \tag{7}$$

TABLE I. Frequencies and polarization of the Peierls-active T_2^+ phonon modes at room temperature. The global prefactor is given by $u^2=(8.26\pm0.02)\times10^{-26}$ kg. The notation is $e_\nu^z(\lambda,\mathbf{q}_0)\equiv e_\nu^z(\lambda)$.

λ	1	2	3	4
$\Omega_\lambda/(2\pi)$	3.12 THz	6.53 THz	11.1 THz	24.6 THz
$ue^z_{\mathrm{Cu}}(\lambda)/\sqrt{m_{\mathrm{Cu}}}$	0.0095	−0.4790	0.7412	−0.0888
$ue^y_{\mathrm{Ge}}(\lambda)/\sqrt{m_{\mathrm{Ge}}}$	−0.4330	−0.5325	−0.3698	−0.2605
$ue^x_{\mathrm{O(2b)}}(\lambda)/\sqrt{m_{\mathrm{O(2)}}}$	−0.6212	0.6581	0.3382	−0.7932
$ue^y_{\mathrm{O(2b)}}(\lambda)/\sqrt{m_{\mathrm{O(2)}}}$	−0.8620	0.1339	0.2021	0.8723

$$P_{\lambda,\mathbf{q}}=i\sqrt{\frac{\hbar\Omega_{\lambda,\mathbf{q}}}{2}}(b^\dagger_{\lambda,-\mathbf{q}}-b_{\lambda,\mathbf{q}}), \tag{8}$$

yields the Hamiltonian usually used in the theoretical treatment of the lattice vibrations

$$H_p=\sum_{\mathbf{q},\lambda}\hbar\Omega_{\lambda,\mathbf{q}}\left(b^\dagger_{\lambda,\mathbf{q}}b_{\lambda,\mathbf{q}}+\frac{1}{2}\right). \tag{9}$$

With the experimentally determined phonon modes $\Omega_{\lambda,\mathbf{q}}$ and shell-model calculations, it is possible to determine the components of the polarization vectors $\mathbf{e}_\nu(\lambda,\mathbf{q})$.[5] At the wave vector of the Peierls instability $\mathbf{q}_0=(\pi/a,0,\pi/c)$, four of the 30 modes correspond to the irreducible representation with the symmetry of the lattice distortion in the spin-Peierls phase, T_2^+ in the notation of Ref. 19. $a=4.8$ Å, $b=8.5$ Å, and $c=2.9$ Å are the lengths of the unit cell in the x, y, and z direction, respectively.

Adapting the lattice-dynamical model presented in Ref. 5, a special effort was made for the description of the spin-Peierls relevant modes by the introduction of additional force constants; details of the lattice-dynamical study will be given elsewhere.[20] The T_2^+ modes are characterized by displacements of the Cu ions along c, of the O(2) sites along a and b, and of the Ge ions along b. The polarization pattern of the four modes as obtained by the shell model are represented in Fig. 2 and given together with their frequencies in Table I. The highest T_2^+ mode corresponds to a Ge-O bond stretching vibration thereby explaining its elevated frequency. The three T_2^+ modes at lower energies posses a common element which consists of the rotation of the O(2)-O(2) edges of the CuO_4 plaquettes in the x-y plane around the c axis. However, only for the lowest mode does this twisting of the CuO_2 ribbons describe the main character of the polarization pattern. The modes at 11 and at 6.5 THz show, in addition, a modulation of the lengths of the O(2)-O(2) edges and a Cu shift parallel c. For the 11 THz mode the displacements of the Cu ions modulate the O(2)-Cu bond distance. The 6.5 THz mode is characterized by a strong modulation of the Cu-O(2)-Cu bond angle (see Fig. 2) which is essential for the magnetic interaction.

For later use we define the matrix $\mathbf{M}$ with the elements given by $e_\nu^\alpha(\lambda,\mathbf{q}_0)/\sqrt{m_\nu}$ extracted from Table I:

TABLE II. Definition of the coupling constants for linear atomic elongations. The two Cu chains running through each unit cell are distinguished by a prime (see Fig. 1). J' is the magnetic coupling constant along the Cu′ chains.

$$g^z_{\mathrm{Cu}}=\frac{\partial J}{\partial r^z_{\mathrm{Cu},\mathbf{n}}}=-\frac{\partial J}{\partial r^z_{\mathrm{Cu},\mathbf{n}+\hat{z}}}=\frac{\partial J'}{\partial r^z_{\mathrm{Cu}',\mathbf{n}}}$$

$$g^y_{\mathrm{Ge}}=\frac{\partial J}{\partial r^y_{\mathrm{Ge},\mathbf{n}}}=-\frac{\partial J}{\partial r^y_{\mathrm{Ge}',\mathbf{n}-\hat{y}}}=-\frac{\partial J'}{\partial r^y_{\mathrm{Ge},\mathbf{n}}}$$

$$g^{x,y}_{\mathrm{O(2a)}}=\frac{\partial J'}{\partial r^{x,y}_{\mathrm{O(2a)},\mathbf{n}}}=-\frac{\partial J'}{\partial r^{x,x}_{\mathrm{O(2a)}',\mathbf{n}}}=-\frac{\partial J'}{\partial r^{x,y}_{\mathrm{O(2a)}',\mathbf{n}-\hat{y}}}$$

$$g^{x,y}_{\mathrm{O(2b)}}=\frac{\partial J}{\partial r^{x,y}_{\mathrm{O(2b)},\mathbf{n}}}=-\frac{\partial J}{\partial r^{x,y}_{\mathrm{O(2b)}',\mathbf{n}}}=-\frac{\partial J}{\partial r^{x,y}_{\mathrm{O(2b)}',\mathbf{n}-\hat{y}}}$$

$$\mathbf{M}=\begin{pmatrix}0.03&-1.67&2.58&-0.31\\-1.51&-1.85&-1.29&-0.91\\-2.16&2.29&1.18&-2.76\\-3.00&0.47&0.70&3.04\end{pmatrix}\frac{10^{12}}{\sqrt{kg}}. \tag{10}$$

The static distortion in the spin-Peierls phase at $T=4$ K also has been determined.[15] We define a corresponding four-dimensional vector:

$$\langle\mathbf{r}\rangle_{T=4\ \mathrm{K}}=\begin{pmatrix}\langle r^z_{\mathrm{Cu}}\rangle\\\langle r^y_{\mathrm{Ge}}\rangle\\\langle r^x_{\mathrm{O(2b)}}\rangle\\\langle r^y_{\mathrm{O(2b)}}\rangle\end{pmatrix}=10^{-2}\begin{pmatrix}0.57\\0.08\\-0.95\\-0.65\end{pmatrix}\text{Å}. \tag{11}$$

III. SPIN-PHONON COUPLING TERM

In the spin-phonon coupling term (4) we focus on the NN part for reasons that will become obvious at the end of the section. We include the relevant displacements of the ions directly involved in the Cu-Cu superexchange path determining J and only those coupling constants where the ions actually show displacements in the Peierls-active modes. The apex ''O(1)'' atoms are not displaced by those modes at the appropriate wave vector $\mathbf{q}_0$. We have to consider two copper ions in adjacent unit cells along the c direction, two germanium sites, and two oxygen atoms surrounding a Cu-Cu bond. The notation introduced is shown in Fig. 1, the two O(2) oxygen atoms per formula unit are denoted O(2a) and O(2b). There are two formula units per unit cell which we distinguish by a prime.

The relevant coupling constants for the linear atomic elongations are shown in Table II. The effective spin-phonon coupling Hamiltonian is

$$H_{sp}^{\mathrm{NN}}=\sum_{\mathbf{n}}\ [g^{z}_{\mathrm{Cu}}(r^{z}_{\mathrm{Cu},\mathbf{n}}-r^{z}_{\mathrm{Cu},\mathbf{n}+\hat{z}})-g^{y}_{\mathrm{Ge}}(r^{y}_{\mathrm{Ge}',\mathbf{n}-\hat{y}}-r^{y}_{\mathrm{Ge},\mathbf{n}})-g^{x}_{\mathrm{O(2b)}}(r^{x}_{\mathrm{O(2b)}',\mathbf{n}-\hat{y}}-r^{x}_{\mathrm{O(2b)},\mathbf{n}})$$

$$-g^{y}_{\mathrm{O(2b)}}(r^{y}_{\mathrm{O(2b)}',\mathbf{n}-\hat{y}}-r^{y}_{\mathrm{O(2b)},\mathbf{n}})]\mathbf{S}_{\mathbf{n}}\cdot\mathbf{S}_{\mathbf{n}+\hat{z}}+\sum_{\mathbf{n}}\ [g^{z}_{\mathrm{Cu}}(r^{z}_{\mathrm{Cu}',\mathbf{n}}-r^{z}_{\mathrm{Cu}',\mathbf{n}+\hat{z}})-g^{y}_{\mathrm{Ge}}(r^{y}_{\mathrm{Ge},\mathbf{n}}-r^{y}_{\mathrm{Ge}',\mathbf{n}})+g^{x}_{\mathrm{O(2a)}}(r^{x}_{\mathrm{O(2a)},\mathbf{n}}-r^{x}_{\mathrm{O(2a)}',\mathbf{n}})$$

$$+g^{y}_{\mathrm{O(2a)}}(r^{y}_{\mathrm{O(2a)},\mathbf{n}}-r^{y}_{\mathrm{O(2a)}',\mathbf{n}})]\ \ \mathbf{S}'_{\mathbf{n}}\cdot\mathbf{S}'_{\mathbf{n}+\hat{z}}. \tag{12}$$

The two sums correspond to the two Cu chains running through each unit cell.

The symmetry of the Hamiltonian (12) allows for some simplifications. First of all we use the equivalence of coupling to the O(2a) and O(2b) displacements (see Fig. 1):

$$g^{x}_{\mathrm{O}(2)}=g^{x}_{\mathrm{O(2b)}}=g^{x}_{\mathrm{O(2a)}}, \tag{13}$$

$$g^{y}_{\mathrm{O}(2)}=g^{y}_{\mathrm{O(2b)}}=-g^{y}_{\mathrm{O(2a)}}. \tag{14}$$

From the symmetry of the T_2^+ modes (see Fig. 2) we see that the O(2)-y components are in phase, i.e., $r^{y}_{\mathrm{O(2a)},\mathbf{n}}=r^{y}_{\mathrm{O(2b)},\mathbf{n}}=r^{y}_{\mathrm{O}(2),\mathbf{n}}$, while the x components exhibit an antiphase shift: $-r^{x}_{\mathrm{O(2a)},\mathbf{n}}=r^{x}_{\mathrm{O(2b)},\mathbf{n}}=r^{x}_{\mathrm{O}(2),\mathbf{n}}$.

As indicated in Fig. 1 we then cut the unit cell along the y axis in half separating the ions labeled ''prime'' from those without a label.

$$r^{\alpha}_{\nu',\mathbf{n}}\rightarrow -r^{\alpha}_{\nu,\mathbf{n}+\hat{y}/2}, \tag{15}$$

$$\mathbf{S}'_{\mathbf{n}}\cdot\mathbf{S}'_{\mathbf{n}+\hat{z}}\rightarrow\mathbf{S}_{\mathbf{n}+\hat{y}/2}\cdot\mathbf{S}_{\mathbf{n}+\hat{y}/2+\hat{z}}. \tag{16}$$

The change of sign of the coordinates accounts for the antiphase elongation of the two types of ions in the Peierls-active modes at the wave vector of the instability $\mathbf{q}=\mathbf{q}_0=(\pi/a,0,\pi/c)$. Resummation $\mathbf{n}\rightarrow\mathbf{l}$ over all the new cells, i.e., twice as many with a new cell length $b/2$ in the y direction, yields

$$H_{sp}^{\mathrm{NN}}=\sum_{\mathbf{l}}\ [g^{z}_{\mathrm{Cu}}(r^{z}_{\mathrm{Cu},\mathbf{l}}-r^{z}_{\mathrm{Cu},\mathbf{l}+\hat{z}})+g^{y}_{\mathrm{Ge}}(r^{y}_{\mathrm{Ge},\mathbf{l}-\hat{y}}+r^{y}_{\mathrm{Ge},\mathbf{l}})$$

$$+g^{x}_{\mathrm{O}(2)}(r^{x}_{\mathrm{O}(2),\mathbf{l}-\hat{y}}+r^{x}_{\mathrm{O}(2),\mathbf{l}})$$

$$+g^{y}_{\mathrm{O}(2)}(r^{y}_{\mathrm{O}(2),\mathbf{l}-\hat{y}}+r^{y}_{\mathrm{O}(2),\mathbf{l}})]e^{i\pi l_y}\ \ \mathbf{S}_{\mathbf{l}}\cdot\mathbf{S}_{\mathbf{l}+\hat{z}}. \tag{17}$$

The overall change of sign in the first sum with respect to the second in Eq. (12) has been incorporated in the phase factor $e^{i\pi l_y}$. This change of sign translates into the antiphase shift of the spin-Peierls ordering between neighboring Cu chains in the y direction.

Now we substitute the displacements $r^{\alpha}_{\nu,\mathbf{l}}$ with the $\mathbf{q}$-space normal coordinates (5). For clarity we introduce the abbreviation

$$S_{-\mathbf{q}}:=\sum_{\mathbf{l}}\ e^{i\mathbf{q}\mathbf{R}_{\mathbf{l}}}e^{i\pi l_y}\mathbf{S}_{\mathbf{l}}\cdot\mathbf{S}_{\mathbf{l}+\hat{z}} \tag{18}$$

for the Fourier transform of the nearest-neighbor spin-spin correlation operator:

$$H_{sp}^{\mathrm{NN}}=\frac{1}{\sqrt{N}}\sum_{\mathbf{q}}\ S_{-\mathbf{q}}\sum_{\lambda}\ \sqrt{\frac{2\Omega_{\lambda,\mathbf{q}}}{\hbar}}g_{\lambda}(\mathbf{q})Q_{\lambda,\mathbf{q}}. \tag{19}$$

Here the effective normal mode coupling constant

$$\sqrt{\frac{2\Omega_{\lambda,\mathbf{q}}}{\hbar}}g_{\lambda}(\mathbf{q}):=(1-e^{iq^{z}c})g^{z}_{\mathrm{Cu}}\frac{\mathrm{e}^{z}_{\mathrm{Cu}}(\lambda,\mathbf{q})}{\sqrt{m_{\mathrm{Cu}}}}+(e^{-iq^{y}b/2}+1)$$

$$\times\left(g^{y}_{\mathrm{Ge}}\frac{\mathrm{e}^{y}_{\mathrm{Ge}}(\lambda,\mathbf{q})}{\sqrt{m_{\mathrm{Ge}}}}+g^{x}_{\mathrm{O}(2)}\frac{\mathrm{e}^{x}_{\mathrm{O}(2)}(\lambda,\mathbf{q})}{\sqrt{m_{\mathrm{O}(2)}}}\right.$$

$$\left.+g^{y}_{\mathrm{O}(2)}\frac{\mathrm{e}^{y}_{\mathrm{O}(2)}(\lambda,\mathbf{q})}{\sqrt{m_{\mathrm{O}(2)}}}\right) \tag{20}$$

was introduced.[21]

The next step is to transform the normal coordinates to boson creation and annihilation operator representation via Eq. (7):

$$H_{sp}^{\mathrm{NN}}=\frac{1}{\sqrt{N}}\sum_{\mathbf{q}}\ S_{-\mathbf{q}}\sum_{\lambda}\ g_{\lambda}(\mathbf{q})(b^{\dagger}_{\lambda,-\mathbf{q}}+b_{\lambda,\mathbf{q}}). \tag{21}$$

This is the representation usually used in theoretical approaches to spin-phonon coupling.[7] Since the polarization vectors are known for $\mathbf{q}_0$ (Table I), Eq. (20) defines the relation between the coupling to the linear atomic deviations g^{α}_{ν} (Table II) and the normal mode coupling constants $g_{\lambda}(\mathbf{q})$.

The NNN exchange term $J_2\mathbf{S}_{\mathbf{l}}\cdot\mathbf{S}_{\mathbf{l}+2\hat{z}}$ leads to a magnetoelastic coupling equivalent to the one for the NN exchange shown in Eq. (17). Including all ionic linear elongations contributing to the Cu-O(2)-O(2)-Cu NNN superexchange path the prefactors in the resulting reciprocal-space coupling constants — compare Eq. (20) — then are $(1-e^{2iq^{z}c})$ for the Cu part and $(1+e^{iq^{z}c})$ for the other ions. The coupling of the J_2 term vanishes at the wave vector of the instability $\mathbf{q}=\mathbf{q}_0=(\pi/a,0,\pi/c)$ and does thus not directly influence the transition. Within the present work we can disregard this contribution.

IV. COUPLING TO BOND ANGLES AND LENGTHS

The two lower Peierls-active modes essentially vary the angles $\eta^{\kappa}=\angle$ [Cu-O(2κ)-Cu] and $\delta^{\kappa}=\angle[\overline{\mathrm{O}(2\kappa)'\text{-O}(2\kappa)}\text{-Ge}]$. Together with the bond lengths $d^{\kappa}_{\mathrm{Cu}}=\overline{\text{Cu-O}(2\kappa)}$ and $d^{\kappa}_{\mathrm{Ge}}=\overline{\text{Ge-O}(2\kappa)}$ they represent the natural set of coordinates of the lattice vibrations in the irreducible group of the T_2^+ modes. The index $\kappa\in\{a,a',b,b'\}$ was introduced to label the position on the different oxygen atoms in the unit cell.

TABLE III. Linear coefficients of the expansion of the angles and bond lengths as a function of the linear atomic elongations, as defined in Eq. (22). The variables $\kappa \in \{a,a',b,b'\}$ and $\theta^\kappa \in \{\eta^\kappa, \delta^\kappa, d^\kappa_{\mathrm{Cu}}, d^\kappa_{\mathrm{Ge}}\}$ are introduced in the text. The last line holds the experimental equilibrium angles and bond lengths (Ref. 15) [$\theta^\kappa = \theta_0 + \Delta\theta^\kappa$, $\Delta\theta^\kappa$ is defined in Eq. (22)].

θ	η	δ	d_{Cu}	d_{Ge}
$\lvert\partial\theta^\kappa/\partial r^z_{\mathrm{Cu}}\rvert$	$0.11\ \frac{\pi}{\text{Å}}$	0	0.76	0
$\lvert\partial\theta^\kappa/\partial r^y_{\mathrm{Ge}}\rvert$	0	$0.11\ \frac{\pi}{\text{Å}}$	0	0.82
$\lvert\partial\theta^\kappa/\partial r^x_{\mathrm{O}(2)}\rvert$	$0.21\ \frac{\pi}{\text{Å}}$	$0.29\ \frac{\pi}{\text{Å}}$	0.54	0.57
$\lvert\partial\theta^\kappa/\partial r^y_{\mathrm{O}(2)}\rvert$	$0.14\ \frac{\pi}{\text{Å}}$	$0.32\ \frac{\pi}{\text{Å}}$	0.36	0.82
θ_0	$0.55\ \pi$	$0.89\ \pi$	1.93 Å	1.73 Å

Introducing the variable $\theta^\kappa \in \{\eta^\kappa, \delta^\kappa, d^\kappa_{\mathrm{Cu}}, d^\kappa_{\mathrm{Ge}}\}$ we can write

$$\Delta J_{\mathbf{l},\mathbf{l}+\hat{z}} = \sum_{\{\theta\}} \frac{\partial J}{\partial \theta^\kappa_{\mathbf{n}}} \Delta\theta^\kappa_{\mathbf{n}} = \sum_{\{\theta\}} g_\theta \sum_\nu \frac{\partial \theta^\kappa_{\mathbf{n}}}{\partial r^\alpha_{\nu,\mathbf{n}}} r^\alpha_{\nu,\mathbf{n}}. \tag{22}$$

Here we defined the coupling constants $g_\theta = (\partial J)/(\partial\theta^\kappa_{\mathbf{n}})$, which are independent of κ. For reasons of translational invariance we can drop the unit-cell index $\mathbf{n}$. The linear coefficients of the Taylor expansions $(\partial\theta^\kappa)/(\partial r^\alpha_\nu)$ at different positions κ in the unit cell all yield the same numerical coefficients but with varying signs. The absolute values of the coefficients are given in Table III.

Considering all the relevant bonds and angles and using the decomposition (22) we can set up a spin-phonon Hamiltonian similar to Eq. (12) in the previous section. By a simple comparison of the coefficients we obtain the transformation matrix between the angular and bond-length coupling constants and the linear atomic deviation coupling constants:

$$\begin{pmatrix} g^z_{\mathrm{Cu}} \\ g^y_{\mathrm{Ge}} \\ g^x_{\mathrm{O}(2)} \\ g^y_{\mathrm{O}(2)} \end{pmatrix} = \begin{pmatrix} -0.22\ \frac{\pi}{\text{Å}} & 0 & -1.52 & 0 \\ 0 & -0.11\ \frac{\pi}{\text{Å}} & 0 & 0.82 \\ 0.21\ \frac{\pi}{\text{Å}} & 0.29\ \frac{\pi}{\text{Å}} & -1.08 & 0.57 \\ -0.14\ \frac{\pi}{\text{Å}} & 0.32\ \frac{\pi}{\text{Å}} & 0.72 & -0.82 \end{pmatrix} \begin{pmatrix} g_\eta \\ g_\delta \\ g^d_{\mathrm{Cu}} \\ g^d_{\mathrm{Ge}} \end{pmatrix}. \tag{23}$$

Together with Eq. (20) we now can determine all coupling constants if any four of the them are known.

V. NORMAL MODE COUPLING CONSTANTS

We now numerically determine the four normal mode coupling constants. We have shown the RPA approach by Cross and Fisher[4] for the Hamiltonian

$$H = J\sum_{\mathbf{l}} \mathbf{S}_{\mathbf{l}}\cdot\mathbf{S}_{\mathbf{l}+\hat{z}} + J_2\sum_{\mathbf{l}} \mathbf{S}_{\mathbf{l}}\cdot\mathbf{S}_{\mathbf{l}+2\hat{z}} + \sum_{\mathbf{q},\lambda} \hbar\Omega_{\lambda,\mathbf{q}}\left(b^\dagger_{\lambda,\mathbf{q}} b_{\lambda,\mathbf{q}} + \frac{1}{2}\right) + \frac{1}{\sqrt{N}}\sum_{\mathbf{q}} S_{-\mathbf{q}} \sum_\lambda g_\lambda(\mathbf{q})(b^\dagger_{\lambda,-\mathbf{q}} + b_{\lambda,\mathbf{q}}) \tag{24}$$

to satisfactorily describe the dynamics of the Peierls-active phonon modes.[7] It consists of the Heisenberg chain (2), the harmonic phonon part (9), and the spin-phonon coupling term (21) all discussed above. We have given an expression for the critical temperature of the spin-Peierls transition[7] which we generalize to the four Peierls-active modes we have to consider herein ($\Omega_{\lambda,\mathbf{q}_0} \equiv \Omega_\lambda$, $g_\lambda(\mathbf{q}_0) \equiv g_\lambda$):[21]

$$k_{\mathrm{B}} T_{\mathrm{SP}} = \left(\frac{2g_1^2}{\hbar\Omega_1} + \frac{2g_2^2}{\hbar\Omega_2} + \frac{2g_3^2}{\hbar\Omega_3} + \frac{2g_4^2}{\hbar\Omega_4}\right)\chi_0. \tag{25}$$

The factor $\chi_0 \approx 0.5$ is a contribution of the static spin-polarization function at the appropriate wave vector. Its value is controversial and we have adopted a mean of the proposed values. Please refer to the discussion in Sec. IX for the details.

A. Ginzburg criterion

The Ginzburg criterion gives an estimate of the temperature range of the critical region in which fluctuations suppress the applicability of mean-field approaches (or RPA). It is obtained through comparing the theoretical correction of Gaussian fluctuations to the specific heat

$$C_p - C_{p,0} = \frac{abc}{16\pi} \frac{T^2_{\mathrm{SP}}}{(T-T_{\mathrm{SP}})^2} \frac{k_{\mathrm{B}}}{\xi_a\xi_b\xi_c} \tag{26}$$

with the experimental jump in the specific heat at the transition.[22] The correlation lengths ξ_a, ξ_b, and ξ_c along the respective crystallographic axes can be obtained from fits to the diffuse x-ray data from Schoeffel *et al.*[23]

$$\xi_a \approx 0.50a[(T-T_{\mathrm{SP}})/T_{\mathrm{SP}}]^{-1/3},$$

$$\xi_b \approx 0.65b[(T-T_{\mathrm{SP}})/T_{\mathrm{SP}}]^{-1/3},$$

$$\xi_c \approx 3.06c[(T-T_{\mathrm{SP}})/T_{\mathrm{SP}}]^{-1/3}.$$

The specific-heat jump has been determined by Lasjaunias *et al.*[24] to be $\Delta C_{\mathrm{exp}} = 0.73 k_{\mathrm{B}}$ at T_{SP} per unit-cell volume. Requiring $C_p - C_{p,0} \ll \Delta C_{\mathrm{exp}}$ we find the Ginzburg criterion to be

$$(T-T_{\mathrm{SP}}) \gg 0.03 T_{\mathrm{SP}} = 0.4\ \mathrm{K}. \tag{27}$$

In accordance with the mean-field approach to the susceptibility by Klümper *et al.*[25] we conclude that beyond a region of 3–4 K around T_{SP} the mean-field theory is reliable.

TABLE IV. Normal mode coupling constants for the four Peierls-active phonon modes at $\mathbf{q}_0$, determined by Eq. (32).

g_1/k_B	g_2/k_B	g_3/k_B	g_4/k_B
−15 K	58 K	−30 K	−12 K

B. Mean-field approach

The transition temperature given for $CuGeO_3$ with 14.1 K, one parameter is fixed through Eq. (25). As we shall discuss now, the others can be estimated from the polarization vectors of the Peierls-active phonon modes and the static distortion in the dimerized phase at 4 K also given by Braden *et al.*[15] For the fixed wave vector of the Peierls instability $\mathbf{q}_0$ we can derive from expressions (5) and (7) a relation between a static lattice distortion $\langle r_\nu^\alpha \rangle$ and the expectation values of the displacement of the eigenmodes out of the harmonic equilibrium $\langle b_{\lambda,\mathbf{q}_0} \rangle$:

$$\langle r_\nu^\alpha \rangle = \frac{\langle r^\alpha_{\mathbf{q}_0,\nu} \rangle}{\sqrt{N}} = \sum_\lambda \frac{e_\nu^\alpha(\lambda,\mathbf{q}_0)}{\sqrt{N m_\nu}} \sqrt{\frac{2\hbar}{\Omega_{\lambda,\mathbf{q}_0}}} \langle b_{\lambda,\mathbf{q}_0} \rangle. \quad (28)$$

Introducing the canonical transformation

$$\tilde{b}_{\lambda,\mathbf{q}} = b_{\lambda,\mathbf{q}} + \frac{1}{\sqrt{N}} \frac{g_\lambda(\mathbf{q})}{\hbar \Omega_{\lambda,\mathbf{q}}} S_{\mathbf{q}} \quad (29)$$

for the Bose annihilation and creation operators $b_{\lambda,\mathbf{q}}$, where $S_{\mathbf{q}}$ was defined by Eq. (18), the Hamiltonian (24) decouples into

$$H = J \sum_{\mathbf{l}} \mathbf{S}_{\mathbf{l}} \cdot \mathbf{S}_{\mathbf{l}+\hat{z}} - \frac{1}{N} \sum_{\lambda \mathbf{q}} \frac{|g_\lambda(\mathbf{q})|^2}{\hbar \Omega_{\lambda,\mathbf{q}}} S_{-\mathbf{q}} S_{\mathbf{q}} + \sum_{\mathbf{q},\lambda} \hbar \Omega_{\lambda,\mathbf{q}} \left(\tilde{b}^\dagger_{\lambda,\mathbf{q}} \tilde{b}_{\lambda,\mathbf{q}} + \frac{1}{2} \right). \quad (30)$$

The operators $\tilde{b}_{\lambda,\mathbf{q}}$ do not satisfy Bose commutation relations and since $[S_{-\mathbf{q}}, \tilde{b}_{\lambda,\mathbf{q}}]_- \neq 0$ the solution of this Hamiltonian is not at all evident. But in a mean-field-like approach we can assume $\langle \tilde{b}_{\lambda,\mathbf{q}} \rangle = 0$ so that from Eq. (29) follows

$$\langle b_{\lambda,\mathbf{q}} \rangle = -\frac{1}{\sqrt{N}} \frac{g_\lambda(\mathbf{q})}{\hbar \Omega_{\lambda,\mathbf{q}}} \langle S_{\mathbf{q}} \rangle. \quad (31)$$

TABLE V. Coupling constants for the linear atomic displacements calculated via Eq. (34) using the values for g_λ from Table IV.

g^z_{Cu}/k_B	g^y_{Ge}/k_B	$g^x_{O(2)}/k_B$	$g^y_{O(2)}/k_B$
−890 K/Å	−110 K/Å	400 K/Å	−91 K/Å

TABLE VI. Coupling constants for the angles and bond lengths calculated via Eq. (23) using the values for g_ν^α from Table V.

g_η/k_B	g_δ/k_B	g^d_{Cu}/k_B	g^d_{Ge}/k_B
15 K/deg	1.5 K/deg	180 K/Å	−96 K/Å

The mean-field ansatz is reasonable here, since we are interested in temperatures of 4 K which is far from the critical region and the dimerization is as good as saturated.[2]

C. Values

With Eq. (28) and (31) we are left with a set of linear equations. The values of the frequencies Ω_λ are given in Table I, the polarization vectors $e_\nu^\alpha(\lambda,\mathbf{q}_0)$ enter via the matrix $\mathbf{M}$ defined in Eq. (10), and $\langle \mathbf{r} \rangle_{T=4\ K}$ is given in Eq. (11):

$$\langle \mathbf{r} \rangle_{T=4\ K} = -\frac{\langle S_{\mathbf{q}_0} \rangle}{N} \sqrt{\frac{2}{\hbar}} \mathbf{M} \begin{pmatrix} g_1/\sqrt{\Omega_1^3} \\ g_2/\sqrt{\Omega_2^3} \\ g_3/\sqrt{\Omega_3^3} \\ g_4/\sqrt{\Omega_4^3} \end{pmatrix}. \quad (32)$$

The solution of the equations gives the coupling constants as a function of $N/\langle S_{\mathbf{q}_0} \rangle$. The latter is then determined by the critical temperature $T_{SP} = 14.1$ K via Eq. (25):

$$\frac{\langle S_{\mathbf{q}_0} \rangle}{N} = \frac{1}{N} \sum_{\mathbf{l}} (-1)^{l_x + l_y + l_z} \langle \mathbf{S}_{\mathbf{l}} \cdot \mathbf{S}_{\mathbf{l}+\hat{z}} \rangle = 0.59. \quad (33)$$

For a spin-1/2 system with two Cu chains per unit cell we have $\langle S_{\mathbf{q}_0} \rangle / N \leqslant 0.75$ where 0.75 is reached in the fully dimerized state. In the uniform Heisenberg case $\langle S_{\mathbf{q}_0} \rangle / N = 0$.

In Table IV we show the calculated coupling constants of the spin system to the Peierls-active eigenmodes of the lattice at the wave vector of the instability $\mathbf{q}_0$. The signs are such that all contributions in the spin-phonon coupling term in the Hamiltonian (24) are negative when the phonon modes are macroscopically occupied as determined via Eq. (28) in Sec. VII A. The mode at $\Omega_2/(2\pi) = 6.5$ THz is dominant, by its symmetry it essentially varies the angles η. This will be reflected in the corresponding coupling constant discussed below.

Note that the influence on the transition temperature of the lowest $\Omega_1/(2\pi) = 3.1$ THz mode is as important as that of $\Omega_3/(2\pi) = 11$ THz, because of the frequencies in the denominator of Eq. (25).

VI. MICROSCOPIC COUPLING CONSTANTS

The numerical values of the normal mode coupling constants thus given, the microscopic coupling constants can be determined. Using the matrix (10) we rewrite expression (20) for $\mathbf{q} = \mathbf{q}_0$ as

TABLE VII. Variation of J with the variation of the angles. Note that in our notation there are two angles η^κ and two angles δ^κ contributing each to the Cu-Cu superexchange path (see Fig. 1).

Method (Reference)	$\frac{\partial J}{J\partial\eta^\kappa}$	$\frac{\partial J}{J\partial\delta^\kappa}$
Harm. theory and mean field (this paper)	$10\%\ \frac{1}{\text{deg}}$	$1\%\ \frac{1}{\text{deg}}$
Microscopic superexchange (Ref. 14)	$\geqslant 8\%\ \frac{1}{\text{deg}}$	$\geqslant 0.3\%\ \frac{1}{\text{deg}}$
Microscopic superexchange (Ref. 15)	$22\%\ \frac{1}{\text{deg}}$	$0.6\%\ \frac{1}{\text{deg}}$
Pressure vs. magnetostriction (Ref. 17)	$\sim 5\%\ \frac{1}{\text{deg}}$	$\sim 0.5\%\ \frac{1}{\text{deg}}$

$$\mathbf{M}^{\mathrm{T}}\begin{pmatrix} g^z_{\mathrm{Cu}} \\ g^y_{\mathrm{Ge}} \\ g^x_{\mathrm{O}(2)} \\ g^y_{\mathrm{O}(2)} \end{pmatrix} = \frac{1}{\sqrt{2\hbar}}\begin{pmatrix} g_1\sqrt{\Omega_1} \\ g_2\sqrt{\Omega_2} \\ g_3\sqrt{\Omega_3} \\ g_4\sqrt{\Omega_4} \end{pmatrix}, \tag{34}$$

and compute the coupling to the linear atomic elongations. Then we calculate the angular and bond length couplings using Eq. (23). The resulting values are given in Tables V and VI, respectively.

The results allow for some immediate conclusions:

(i) The coupling to η, i.e., g_η, is the dominant contribution.

(ii) The signs of the coupling constants are correct, J increases with increasing angles and decreasing O(2)-Ge bond length. The positive value of g^d_{Cu} indicates that the ferromagnetic exchange is weakened more than the antiferromagnetic exchange when stretching the O(2)-Cu bond. This is consistent with the net ferromagnetic exchange of the O(2)-Cu plaquettes without the germanium side group predicted by Geertsma and Khomskii.[14]

(iii) Variation of the coupling constants shows g_1 to couple mainly to the angles δ, g_2 to η, and g_3 and g_4 to be almost entirely bond stretching.[5] While the results for g_η and g_δ are robust under variation of the parameters, the values of g^d_{Cu} and g^d_{Ge} are less fixed within the accuracy of our approach.

(iv) From magnetostriction data Büchner *et al.*[17] expect the influence of the Cu-O(2)-Cu angle η on the magnetic exchange to be of the order of $2\partial J/(J\partial\eta^\kappa)\approx 10\%$ per degree, and for the O(2)-O(2)-Ge angle their value is $2\partial J/(J\partial\delta^\kappa)\approx 1\%$. For $J/k_{\mathrm{B}}=150$ K we obtain about twice the values (see Table VII).

(v) Comparing g^d_{Ge} and g^y_{Ge} shows the effect of the germanium elongation on the magnetic exchange to be due mainly to the stretching of the O(2)-Ge bond. The contribution of the Ge side group to the magnetic exchange should depend on the O(2)-O(2)-Ge angle as $J_{\mathrm{side}}\sim\cos\delta$. Therefore, the angle $\delta^\kappa\approx 160°=0.89\pi$ being close to π, the angular dependency of J on δ is quite small in spite of the large entire side-group effect, which is of similar magnitude as that of the CuO_4 plaquette elongation.[14,15]

(vi) Two groups analyzed the structural dependence of the superexchange within similar microscopic models. Geertsma and Khomskii[14] obtained $J/k_{\mathrm{B}}=135$ K and found $2\partial J_{\mathrm{geo}}/(J\partial\eta^\kappa)\approx 16\%$ and $2\partial J_{\mathrm{geo}}/(J\partial\delta^\kappa)\approx 0.6\%$ per degree. These values only accout for the ''geometrical'' contribution and are thus lower bounds. Braden *et al.*[15] found $J/k_{\mathrm{B}}=160$ K and gave $2\partial J/(J\partial\eta^\kappa)\approx 44\%$ and $2\partial J/(J\partial\delta^\kappa)\approx 1.1\%$ per degree. The agreement between the microscopic models is affected by the choice of the parameters and the number of orbitals taken into consideration.

A summary of the values obtained in the different approaches is given in Table VII.

VII. STATIC DISTORTION

The microscopic coupling constants given, we can directly calculate the effect of static distortions of the lattice geometry on the magnetic exchange.

A. Dimerization

Using the static displacements of the ions in the spin-Peierls (SP) phase at $T=4$ K,[15] one may calculate the alternation of the magnetic exchange usually used in mean-field approaches to the spin-phonon coupling, i.e.,

$$H_{\mathrm{MF}}=J\sum_{l_z}\left[1+(-1)^{l_z}\delta_J\right]\mathbf{S}_{l_z}\cdot\mathbf{S}_{l_z+1}. \tag{35}$$

This is achieved by substituting in the spin-phonon coupling term (17) the atomic displacements by their expectation values $r^\alpha_{\nu,\mathbf{l}}\rightarrow(-1)^{l_z+l_x}\langle r^\alpha_\nu\rangle_{T=4\ \mathrm{K}}$ and comparing the resulting $\langle H^{\mathrm{NN}}_{sp}\rangle_{T=4\ \mathrm{K}}$ with Eq. (35). Equivalently one can calculate $\langle H^{\mathrm{NN}}_{sp}\rangle_{T=4\ \mathrm{K}}$ by using the static angular and bond length deviations[15] yielding the same results.

We find $\delta_J J/k_{\mathrm{B}}=17$ K or $\delta_J\approx 0.11$ ($J/k_{\mathrm{B}}=150$ K). By solving the system of linear equations defined by Eq. (28) for $\mathbf{q}=\mathbf{q}_0$, the expectation values $\langle b_\lambda\rangle/\sqrt{N}$ have been determined to be 0.061, -0.11, 0.034, and 0.006 for $\lambda=1$, 2, 3, and 4, respectively. The elastic energy per unit cell of the spin-Peierls distortion at $T\sim 4$ K then is given by

TABLE VIII. Exchange alternation in $J[1+(-1)^{l_z}\delta_J]$.

Method (Reference)	δ_J
Harmonic theory and mean field (This paper)	0.11
Macroscopic occupation of T_2^+ modes (This paper)	>0.04
Microscopic superexchange (Refs. 14,15)	0.07 to 0.2
Dynamic phonons and experimental gap (Ref. 17)	~ 0.05
Static phonons and experimental gap (Refs. 11,12)	0.01 to 0.03
Coupled chains (Ref. 16)	0.01 to 0.12

$$\frac{\langle H_p\rangle}{N k_B}=\sum_\lambda \frac{\hbar\Omega_\lambda}{N k_B}\langle b_\lambda\rangle^2=5\mathrm{K}. \tag{36}$$

This energy loss has to be compensated by the spin system. Considering that the maximum gain of magnetic energy is reached in the fully dimerized case with $0.375\delta_J J$ per Cu ion, we find a lower boundary for the dimerization of $\delta_J > 0.044$. Including a NNN term in Eq. (35) with $J_2/J = 0.241$ as studied by Chitra *et al.*[13] using a density matrix renormalization group (DMRG) approach we find $\delta_J \geqslant 0.078$.

Our result is within a factor of 2 of the values obtained by using $\partial J/\partial\eta$ and $\partial J/\partial\delta$ obtained from the magnetostriction results[17] and from the microscopic models.[14,15] All other published estimates of the dimerization result from an analysis of the magnetic excitation spectra observed by inelastic neutron or Raman scattering. Most of these estimates are based on the static dimerized Hamiltonian (35) (Refs. 11,12) and yield dimerization values much smaller than the one reported here (see Table VIII). Augier and Poilblanc[26] as well as Wellein *et al.*[27] extend the static model by coupling to dynamical phonons which reduces the magnetic gap by lowering the effective lattice distortion acting on the spin system.[17] The derivation of their model and the significance of the phonon dynamics are more closely discussed in Sec. VIII. Introducing interchain coupling may further suppress the spin gap.[28] For an extensive discussion see Ref. 16.

All methods incorporate more or less crude approximations to the real physical situation leaving the question of the true value of δ_J unanswered. Our lower boundary should be rather reliable though. The values obtained in the different approaches are given in Table VIII for comparison.

B. Pressure

Bräuninger *et al.*[29] and Braden *et al.*[20] have investigated the pressure dependence of the angles and bond lengths in $CuGeO_3$ under hydrostatic pressure. The linearity of the pressure dependence is reasonable for pressures <2 GPa. The values for the pressure gradients obtained from Ref. 20 are shown in Table IX.

Regarding the partial derivative of the exchange integral $\partial J_\theta/\partial p=(\partial J/\partial\theta)(\partial\theta/\partial p)$ we find immediately the pressure gradients of the different angular and bond length contributions to J as given in Table IX.

Considering all four contributions, we obtain the total variation of the antiferromagnetic exchange:

$$\frac{\partial J}{\partial p}=2\frac{\partial J_\eta}{\partial p}+2\frac{\partial J_\delta}{\partial p}+2\frac{\partial J_{\mathrm{Ge}}}{\partial p}+4\frac{\partial J_{\mathrm{Cu}}}{\partial p}=-9\ \frac{k_B\mathrm{K}}{\mathrm{GPa}}. \tag{37}$$

TABLE IX. Linear pressure gradients of angles and bond lengths from experimental data in Ref. 20 (top) and the resulting theoretical pressure gradients $\partial J_\theta/\partial p=(\partial J/\partial\theta)(\partial\theta/\partial p)$ (bottom). The values for $\partial J/\partial\theta$ are given in Table VI.

θ	η	δ	d_{Cu}	d_{Ge}
$\frac{\partial\theta^\kappa}{\partial p}$	$-0.16\ \frac{\mathrm{deg}}{\mathrm{GPa}}$	$-1.3\ \frac{\mathrm{deg}}{\mathrm{GPa}}$	$-0.0012\ \frac{\text{Å}}{\mathrm{GPa}}$	$-0.0033\ \frac{\text{Å}}{\mathrm{GPa}}$
$\frac{\partial J_\theta}{\partial p}$	$-2.5\ \frac{k_B\mathrm{K}}{\mathrm{GPa}}$	$-1.9\ \frac{k_B\mathrm{K}}{\mathrm{GPa}}$	$-0.22\ \frac{k_B\mathrm{K}}{\mathrm{GPa}}$	$0.32\ \frac{k_B\mathrm{K}}{\mathrm{GPa}}$

For $J/k_B=150$ K this value corresponds to $\partial J/(J\partial p)\approx -6\%$ per GPa. The pressure dependency of the magnetic susceptibility is directly related to the magnetostriction. A value of $-\partial\chi/(\chi\partial p)\sim\partial J/(J\partial p)\approx -8\%$ per GPa was obtained after averaging the uni-axial components.[8,30] Takahashi *et al.*[9] have measured the pressure dependence of the Curie constant C by fitting a Curie-Weiss law to the high-temperature tail of the magnetic susceptibility. Assuming $C\sim 1/J$ one can estimate a value of about $\partial J/(J\partial p)\approx -7\%$ per GPa. Nishi and co-workers[10] compared fits to the dispersion of the lowest triplet excitations at different pressures. They assume the ratio between the exchange J and next-nearest-neighbor exchange J_2 with a value of $J_2/J\approx 0.25$ which does alter under pressure, and found $\partial J/(J\partial p)\approx -10\%$ per GPa. In contrast to that Fabricius *et al.*[30] found that J_2 does not alter under pressure. Then the result from Nishi's analysis is corrected to $\partial J/(J\partial p)\approx -8\%$ per GPa. A summary of the values is given in Table X showing their consistency.

C. Thermal expansion and spontaneous strain

In a harmonic lattice the coefficients of linear thermal expansion $\alpha=(\partial L)/(L\partial T)_p$ vanish. Here L is the length of the crystal in a given spatial direction. Anharmonic contributions result in temperature-dependent phonon frequencies which in turn yield finite values for α. The coefficient of thermal expansion is linked to the specific heat via the (temperature dependent) Grüneisen parameter. This implies in the limiting cases $T\to 0:\alpha\sim T^3$ and $T\gg\Theta_D:\alpha\sim$ constant, where Θ_D is the Debye temperature.[31]

The thermal expansion in $CuGeO_3$ can be attributed to two effects: the usual anharmonic behavior described above and anomalies due to the spin-phonon coupling.[32,33] The coefficient of linear thermal expansion of the c axis in $CuGeO_3$ has a negative sign between T_{SP} and $T\sim 200$ K. The expansion of the c axis enlarges J via the angle η. The spin system then gains energy when the temperature is lowered to $T\sim J$ by driving the anomaly.[34] A rough quantitative estimation can be extracted from the analysis of the temperature dependence of the herein considered bond lengths and angles given by Braden *et al.*[32] Their temperature dependence between 295 K and 20 K is close to linear and presented in Table XI. Summing up the different contributions equivalently to Eq. (37) yields $\partial J/(J\partial T)\approx -2.6\%$ per 250 K ($J/k_B=150$ K). This effect is a superposition of the normal thermal expansion with positive $\partial J_{\mathrm{norm}}/(J\partial T)$ and the anomalous effect at

TABLE X. Variation of J with pressure.

Method (Reference)	$\frac{\partial J}{J\partial p}$
Harmonic theory and mean field (this paper)	$-6\%\ \frac{1}{\text{GPa}}$
Susceptibility via magnetostriction (Ref. 8)	$-8\%\ \frac{1}{\text{GPa}}$
Curie-Weiss fit to the susceptibility (Ref. 9)	$-7\%\ \frac{1}{\text{GPa}}$
Fit to the triplet dispersion (Ref. 10)	-8 to $-10\%\ \frac{1}{\text{GPa}}$

low temperature which can be estimated by $\partial J_{\text{an}}/(J\partial T) \leqslant 2\partial J_{\eta}/(J\partial T) = -4.1\%$ per 250 K.

As the crystal undergoes the SP transition spontaneous strain appears along all three orthorhombic directions.[35,33] The strain couples different T_2^+ modes[36] and gives a correction to Eq. (32) which we now show to be unimportant. The elastic energy per unit cell related to the spontaneous strain at $T\sim 4$ K can be estimated from the elastic constants. The diagonal elastic constants were taken from the ultrasound study by Poirier *et al.*,[37] and off-diagonal terms were calculated with the lattice-dynamical model[20] as shown in Table XII using standard notation.[31] With the values for the strain ϵ_i given by Winkelmann *et al.*[33] we find

$$\frac{E_{\text{strain}}}{k_{\text{B}}} = \frac{a\cdot b\cdot c}{2k_{\text{B}}} \sum_{i,j=1,2,3} \epsilon_i C_{ij} \epsilon_j = 7\times 10^{-4}\ \text{K}. \tag{38}$$

Note that the strain components $\epsilon_4 = \epsilon_5 = \epsilon_6$ vanish, since the orthorhombicity is conserved. The elastic energy involved in the strain is four orders of magnitude smaller than the elastic energy of the dimerization given in Eq. (36).

Note that the components of the spontaneous strain[33] have the opposite sign compared with the anomalies of the thermal expansion[5] discussed above. The spontaneous strain may thus be interpreted as a relaxation of the latter when the spin system changes its character at the spin-Peierls transition. The relaxation is of the order of 1%.

TABLE XI. Experimental linear temperature gradients of angles and bond lengths from Ref. 32 (top) and the resulting theoretical contributions to the temperature dependence of J (bottom) between 20 and 295 K.

θ	η	δ	d_{Cu}	d_{Ge}
$\frac{\partial\theta^{\kappa}}{\partial T}$	$-0.2\ \frac{\text{deg}}{250\ \text{K}}$	$0.6\ \frac{\text{deg}}{250\ \text{K}}$	$0.0002\ \frac{\text{Å}}{250\ \text{K}}$	$-0.002\ \frac{\text{Å}}{250\ \text{K}}$
$\frac{\partial J_{\theta}}{\partial T}$	$-3.1\ \frac{k_{\text{B}}\text{K}}{250\ \text{K}}$	$0.9\ \frac{k_{\text{B}}\text{K}}{250\ \text{K}}$	$0.04\ \frac{k_{\text{B}}\text{K}}{250\ \text{K}}$	$0.2\ \frac{k_{\text{B}}\text{K}}{250\ \text{K}}$

TABLE XII. Experimental uniaxial elastic constants from Ref. 37 (top) and the theoretical elastic constants obtained from the shell model (bottom).

	C_{11}	C_{22}	C_{33}	C_{12}	C_{13}	C_{23}
Expt. (10^{11} dyn/cm^2)	7.4	2.1	33.2			
Theory (10^{11} dyn/cm^2)	8.2	5.0	34.6	3.0	4.0	2.2

VIII. COUPLING CONSTANTS FOR REAL-SPACE NORMAL COORDINATES

In order to obtain real-space expressions we use the Fourier representation of the Bose operators

$$b_{\lambda,\mathbf{q}} = \frac{1}{\sqrt{N}} \sum_{\mathbf{l}} e^{-i\mathbf{q}\mathbf{R}_{\mathbf{l}}} b_{\lambda,\mathbf{l}}. \tag{39}$$

For simplicity we neglect the wave-vector dependence of the frequencies $\Omega_{\lambda} = \Omega_{\lambda,\mathbf{q}_0}$ and of the polarization vectors $e_{\nu}^{\alpha}(\lambda) = e_{\nu}^{\alpha}(\lambda,\mathbf{q}_0)$. The coupling constants $g_{\lambda}(\mathbf{q}_0)$ in Eq. (20) then are divided into

$$\sqrt{\frac{2\Omega_{\lambda}}{\hbar}} g_{\lambda}^{\text{Cu}} = g_{\text{Cu}}^{z} \frac{e_{\text{Cu}}^{z}(\lambda)}{\sqrt{m_{\text{Cu}}}}, \tag{40}$$

$$\sqrt{\frac{2\Omega_{\lambda}}{\hbar}} g_{\lambda}^{\text{loc}} = g_{\text{Ge}}^{y} \frac{e_{\text{Ge}}^{y}(\lambda)}{\sqrt{m_{\text{Ge}}}} + g_{\text{O(2)}}^{x} \frac{e_{\text{O(2)}}^{x}(\lambda)}{\sqrt{m_{\text{O(2)}}}} + g_{\text{O(2)}}^{y} \frac{e_{\text{O(2)}}^{y}(\lambda)}{\sqrt{m_{\text{O(2)}}}}. \tag{41}$$

Transforming the Hamiltonian (24) via Eq. (39) we obtain in real space

$$\begin{aligned} H_{\text{r}} = & \sum_{\lambda,\mathbf{l}} \hbar\Omega_{\lambda} \left(b_{\lambda,\mathbf{l}}^{\dagger} b_{\lambda,\mathbf{l}} + \frac{1}{2} \right) + J \sum_{\mathbf{l}} \mathbf{S}_{\mathbf{l}} \cdot \mathbf{S}_{\mathbf{l}+1} \\ & + \sum_{\lambda,\mathbf{l}} (-1)^{l_y} [g_{\lambda}^{\text{Cu}} (b_{\lambda,\mathbf{l}}^{\dagger} + b_{\lambda,\mathbf{l}} - b_{\lambda,\mathbf{l}+\hat{z}}^{\dagger} - b_{\lambda,\mathbf{l}+\hat{z}}) \\ & + g_{\lambda}^{\text{loc}} (b_{\lambda,\mathbf{l}}^{\dagger} + b_{\lambda,\mathbf{l}} + b_{\lambda,\mathbf{l}+\hat{y}}^{\dagger} + b_{\lambda,\mathbf{l}+\hat{y}})] \mathbf{S}_{\mathbf{l}} \cdot \mathbf{S}_{\mathbf{l}+\hat{z}}. \end{aligned} \tag{42}$$

The coupling constants are given in Table XIII. This result implies that the oxygen and germanium displacements are of the same importance for the spin-phonon coupling as the copper elongation.

Motivated by the symmetry of the Peierls-active phonon modes an effective onedimensional model can be obtained by restricting the sum to a single chain. The Fourier transform of the one-dimensional model derived from Eq. (42) shows the different q dependences ($q \equiv q^z$) of the copper and the local term.

TABLE XIII. Coupling constants to real-space normal modes obtained from Eqs. (40) and (41).

λ	1	2	3	4
$g_{\lambda}^{\text{Cu}}/k_{\text{B}}$	-0.5 K	17 K	-20 K	1.6 K
$g_{\lambda}^{\text{loc}}/k_{\text{B}}$	-7.2 K	12 K	4.8 K	-7.5 K

$$H_{1D}=\sum_{\lambda,q}\hbar\Omega_\lambda\left(b^\dagger_{\lambda,q}b_{\lambda,-q}+\frac{1}{2}\right)+J\sum_{l_z}\mathbf{S}_{l_z}\cdot\mathbf{S}_{l_z+1}$$
$$+\sum_{\lambda,q}\frac{g_{\lambda 1D}(q)}{\sqrt{N}}(b^\dagger_{\lambda,-q}+b_{\lambda,q})\sum_{l_z}e^{iqR_{l_z}}\mathbf{S}_{l_z}\cdot\mathbf{S}_{l_z+1}. \tag{43}$$

Here we defined the 1D coupling constant

$$g_{\lambda 1D}(q)=(1-e^{iqc})g^{\mathrm{Cu}}_\lambda+2g^{\mathrm{loc}}_\lambda. \tag{44}$$

Several studies[26,27,6,34] have been carried out using real-space Hamiltonians in the form of Eq. (42) reduced to a one-dimensional model. Usually a single-mode Hamiltonian, only keeping the local term is considered, i.e., in their notation $2g^{\mathrm{loc}}_1\equiv g$, while the other coupling constants are set to zero. Considering g^{Cu}_2, g^{loc}_2, and g^{loc}_1 being of the same order of magnitude, this simplification should only yield qualitative results.

Yet, these treatments include the dynamics of the phonons. The significance of the latter can be estimated from the size of the zero-point motion of the ions. Without the negligible contribution from the macroscopic occupation (Sec. VII A) the fluctuations of the T^+_2 modes at $T=0$ can be obtained from Eq. (5) using the approximation of dispersionless phonons introduced above:

$$\overline{\langle(r^\alpha_\nu)^2\rangle}=\frac{1}{N}\sum_{\mathbf{n}}\langle(r^\alpha_{\nu\mathbf{n}})^2\rangle_{T=0}=\sum_\lambda\left(\frac{e^\alpha_\nu(\lambda)}{\sqrt{m_\nu}}\right)^2\frac{\hbar}{2\Omega_\lambda}. \tag{45}$$

The resulting values are $\sqrt{\overline{\langle(r^\alpha_\nu)^2\rangle}}=0.029$, 0.035, 0.048, and 0.053 Å for $r^\alpha_\nu=r^z_{\mathrm{Cu}}$, r^y_{Ge}, $r^x_{\mathrm{O}(2)}$, and $r^y_{\mathrm{O}(2)}$, respectively. They are consistent with the values of the total zero-point fluctuations obtained from the shell model and the neutron-scattering experiments presented in Ref. 32. The zero-point fluctuations are thus a factor of 5 to 10 larger than the static distortions as given in Eq. (11).

On the other hand, the Ginzburg criterion discussed in Sec. V A and the consistency of our results with experimental ones justify our mean-field approach. In accordance with that, Klümper *et al.*[25] show that a variety of physical quantities can be obtained correctly in a mean-field picture. It is beyond the scope of this paper but certainly an interesting question addressed to future studies which quantities are sensitive to the zero-point fluctuations and why.

IX. DISCUSSION OF χ_0

The approach by Cross and Fisher[4,7] gave a value of $\chi_0\approx 0.26$. This value is independent of J because of the scale invariance at $q_c=\pi/c$. The scaling hypothesis is applicable close to the critical point of the spin chain, i.e., in the limit $T\to 0$. Recent DMRG results obtained by Klümper *et al.*[25,38] show a strong temperature dependence of $\chi_0(T/J)$. For $J_2=0$ and $J=120$ K they found $\chi_0(T_{\mathrm{SP}}/J)\approx 0.28$. For $J_2/J=0.241$ and $J=150$ K the parameter attains $\chi_0(T_{\mathrm{SP}}/J)\approx 0.56$, whereas for $J_2/J=0.35$ and $J=160$ K they found $\chi_0(T_{\mathrm{SP}}/J)\approx 1$.

The exact value of J_2 in $CuGeO_3$ has not yet been determined. Fits to the susceptibility for $T>T_{\mathrm{SP}}$ indicate an overcritical J_2,[11,30] but fits to the four-spinon continuum seen by Raman scattering[39] indicate an undercritical J_2. In favor of an undercritical J_2 is also the small binding energy of the singlet bound state for $T<T_{\mathrm{SP}}$, as seen by Raman experiments.[40] Interchain coupling will reduce the value of χ_0 because of an enhancement of the antiferromagnetic correlations.[28]

As can be seen from Eq. (25) our coupling constants scale as $g_\lambda\sim\sqrt{\chi_0}^{-1}$. From the above results follows $1<\sqrt{\chi_0}^{-1}<1.9$ and we adapt the mean value of $\chi_0=0.5$ for our calculations. This value is close to the result for $J_2/J=0.241$. Within the accuracy of our approach we can use $J=150$ K as given by Castilla *et al.*[12] The choice of χ_0 is justified *a posteriori* by the agreement of the results in the literature. Also note that including a NNN term with $J_2/J=0.24$ in Eq. (35) with $\delta_J=0.1$ and using exact diagonalization gives a value of $\Sigma_{l_z}(-1)^{l_z}\langle\mathbf{S}_{l_z}\cdot\mathbf{S}_{l_z+1}\rangle/N=0.57$ per two Cu ions in agreement with the value given in Eq. (33).

Applying hydrostatic pressure the transition temperature grows at a rate of 4.8 K/GPa.[9] In our approach T_{SP} is given by Eq. (25) and depends on the coupling constants g_λ, the frequencies Ω_λ, and the factor χ_0. The coupling constants g_λ in turn depend on the linear derivatives of the magnetic exchange g^α_ν and the polarization vectors, as given in Eq. (20). In a harmonic lattice the phonon frequencies and polarization vectors are independent of pressure. It seems very unlikely that the Peierls-active modes exhibit extremely large negative Grüneisen parameters which would be needed in order to describe the increase of T_{SP} upon pressure via the pressure dependence of the phonon frequencies. The linear coupling constants g^α_ν also are independent of pressure, and since the lattice distortions are rather small,[29,20] we do not expect higher-order contributions to play a crucial role. We must thus conclude the value of χ_0 to be strongly pressure dependent.

Together with the pressure dependence of J_2/J discussed by Fabricius *et al.*,[30] this may explain the shift of T_{SP}.[38] When introducing interchain coupling, prefactors and the functional dependence of the spin-spin correlation function are also altered.[41] The compressibility of the crystal is largest in the *b* direction so that the alternation of the interchain coupling under pressure is another possible origin of the pressure dependence of χ_0 and T_{SP}.

X. SUMMARY

In this paper we have given a detailed analysis of the microscopic magnetoelastic coupling in $CuGeO_3$ which may be easily transferred to other systems. The comparison of several theoretical and experimental approaches yields a satisfactory consistency. Numbers have been given in Table VII for the angular dependence of the magnetic exchange, in

Table VIII for the dimerization, and in Table X for the pressure dependence of the magnetic exchange. The quantitative agreement of course is limited by the uncertainties within experiments and theoretical techniques. Coupling constants for effective one-dimensional real-space model Hamiltonians accessible to numerical studies are given in Table XIII. We have discussed the applicability of static models (Secs. VII A and VIII), and we were able to explain qualitatively the *c*-axis anomaly of the thermal expansion (Sec. VII C).

ACKNOWLEDGMENTS

We are thankful to A. Klümper and R. Raupach for giving us access to results prior to publication and for discussions. We thank W. Weber for discussions and for pointing out the significance of the zero-point fluctuations. We acknowledge fruitful discussions with B. Büchner, H. Fehske, S. Feldkemper, T. Lorenz, U. Löw, and W. Reichardt. The support of the DFG is greatfully acknowledged.

[1] M. Hase, I. Terasaki, and K. Uchinokura, Phys. Rev. Lett. **70**, 3651 (1993).
[2] K. Hirota, G. Shirane, Q.J. Harris, Q. Feng, R.J. Birgeneau, M. Hase, and K. Uchinokura, Phys. Rev. B **52**, 15 412 (1995).
[3] J.E. Lorenzo, K. Hirota, G. Shirane, J.M. Tranquada, M. Hase, K. Uchinokura, H. Kojima, I. Tanaka, and Y. Shibuya, Phys. Rev. B **50**, 1278 (1994).
[4] M.C. Cross and D.S. Fischer, Phys. Rev. B **19**, 402 (1979).
[5] M. Braden, B. Hennion, W. Reichardt, G. Dhalenne, and A. Revcolevschi, Phys. Rev. Lett. **80**, 3634 (1998).
[6] G.S. Uhrig, Phys. Rev. B **57**, R14 004 (1998).
[7] C. Gros and R. Werner, Phys. Rev. B **58**, R14 677 (1998).
[8] B. Büchner, U. Ammerahl, T. Lorenz, W. Brenig, G. Dhalenne, and A. Revcolevschi, Phys. Rev. Lett. **77**, 1624 (1996); T. Lorenz, Ph.D. thesis, University of Köln, 1998.
[9] H. Takahashi, N. Môri, O. Fujita, J. Akimitsu, and T. Matsumoto, Solid State Commun. **95**, 817 (1995).
[10] M. Nishi, O. Fujita, J. Akimitsu, K. Kakurai, and Y. Fujii, Phys. Rev. B **52**, R6959 (1995).
[11] J. Riera and A. Dobry, Phys. Rev. B **51**, 16 098 (1995).
[12] G. Castilla, S. Chakravarty, and V.J. Emery, Phys. Rev. Lett. **75**, 1823 (1995).
[13] R. Chitra, S. Pati, H.R. Krishnamurthy, D. Sen, and S. Ramasesha, Phys. Rev. B **52**, 6581 (1995).
[14] W. Geertsma and D. Khomskii, Phys. Rev. B **54**, 3011 (1996).
[15] M. Braden, G. Wilkendorf, J. Lorenzana, M. An, G.J. McIntyre, M. Behruzi, G. Heger, G. Dhalenne, and A. Revcolevschi, Phys. Rev. B **54**, 1105 (1996).
[16] W. Brenig, Phys. Rev. B **56**, 14 441 (1997), and references therein.
[17] B. Büchner, H. Fehske, A.P. Kampf, and W. Wellein, Physica B **259-261**, 956 (1999).
[18] M. Born and K. Huang, *Dynamical Theory of Crystal Lattices* (Oxford University Press, Oxford, 1968).
[19] H.T. Stokes and D.M. Hatch, *Isotropy Subgroups of the 230 Crystallographic Space Groups* (World Scientific, Singapore, 1988).
[20] M. Braden *et al.* (unpublished).
[21] In the literature the coupling constants often are given with respect to normal coordinates, i.e., in Eq. (19) set $g_{\rm norm} = \sqrt{(2\Omega_{\lambda,\mathbf{q}})/\hbar}\, g_\lambda(\mathbf{q})$. In Eq. (25) the transition temperature then is $T_{\rm SP} \sim g^2_{\rm norm}/\Omega^2$, consistent with the result of Cross and Fisher (Ref. 4).
[22] L.D. Landau and E.M. Lifschitz, *Statistical Mechanics* (Pergamon Oxford, 1968).
[23] J.P. Schoeffel, J.P. Pouget, G. Dhalenne, and A. Revcolevschi, Phys. Rev. B **53**, 14 971 (1996).
[24] J.C. Lasjaunias, P. Monceau, G. Reményi, S. Sahling, G. Dhalenne, and A. Revcolevschi, Solid State Commun. **101**, 677 (1997).
[25] A. Klümper, R. Raupach, and F. Schönfeld, Phys. Rev. B **59**, 3612 (1999).
[26] D. Augier and D. Poilblanc, Eur. Phys. J. B **1**, 19 (1998).
[27] G. Wellein, H. Fehske, A.P. Kampf, Phys. Rev. Lett. **81**, 3956 (1999).
[28] G.S. Uhrig, Phys. Rev. Lett. **79**, 163 (1997).
[29] S. Bräuninger, U. Schwarz, M. Hanfland, T. Zhou, R.K. Kremer, and K. Syassen, Phys. Rev. B **56**, R11 357 (1997).
[30] K. Fabricius, A. Klümper, U. Löw, B. Büchner, T. Lorenz, G. Dhalenne, and A. Revcolevschi, Phys. Rev. B **57**, 1102 (1998).
[31] N.W. Ashcroft and N.D. Mermin, *Solid State Physics* (Saunders College, Fort Worth, 1976).
[32] M. Braden, E. Ressouche, B. Büchner, R. Kessler, G. Heger, G. Dhalenne, and A. Revcolevschi, Phys. Rev. B **57**, 11 497 (1998).
[33] H. Winkelmann, E. Gamper, B. Büchner, M. Braden, A. Revcolevschi, and G. Dhalenne, Phys. Rev. B **51**, 12 884 (1995).
[34] A.W. Sandvik, R.R.P. Singh, and D.K. Campbell, Phys. Rev. B **56**, 14 510 (1997).
[35] T. Lorenz, U. Ammerahl, T. Auweiler, B. Büchner, A. Revcolevschi, and G. Dhalenne, Phys. Rev. B **55**, 5914 (1997).
[36] A.D. Bruce and R.A. Cowley, *Structural Phase Transitions* (Taylor and Francis, London, 1981).
[37] M. Poirier, M. Castonguay, A. Revcolevschi, and G. Dhalenne, Phys. Rev. B **52**, 16 058 (1995).
[38] A. Klümper *et al.* (unpublished).
[39] C. Gros, W. Wenzel, A. Fledderjohann, P. Lemmens, M. Fischer, G. Güntherodt, M. Weiden, C. Geibel, and F. Steglich, Phys. Rev. B **55**, 15 048 (1997).
[40] T. Sekine, H. Kuroe, J-i. Sasaki, Y. Sasago, N. Koide, K. Uchinokura, and M. Hase, J. Phys. Soc. Jpn. **67**, 1140 (1998); G. Bouzerar, A.P. Kampf, and G.I. Japaridze, Phys. Rev. B **58**, 3117 (1998).
[41] H.J. Schulz, Phys. Rev. B **34**, 6372 (1986).